Pure Appl. Chem., Vol. 80, No. 11, pp. 2259–2271, 2008.
doi:10.1351/pac200880112259
© 2008 IUPAC

Development of biodegradable nanosheets as nanoadhesive plaster*

Shinji Takeoka[1,2,‡], Yosuke Okamura[1], Toshinori Fujie[1], and Yoshihito Fukui[1]

[1]Department of Life Science and Medical Bioscience, Graduate School of Advanced Science and Engineering, Waseda University, Tokyo, 169-8555, Japan; [2]Consolidated Research Institute for Advanced Science and Medical Care, Waseda University, Tokyo, 169-8555, Japan

Abstract: Sheet-shaped carriers having both obverse and reverse surfaces (thus, a large contact area for targeting a site and adhesive properties without any chemical cross-linker onto tissue surface) have several advantages as surgical dressings. These advantages include active targeting over spherically shaped carriers, which thus have an extremely small contact area for targeting sites. Here, we propose a novel methodology for preparation of a free-standing, ultra-thin, and biocompatible polymer nanosheet having heterosurfaces, fabricated through macromolecular assembly. In the context of biomedical applications, the targeted properties include injectable sheet-shaped drug carriers having precisely controlled size by exploiting micropatterned substrate, and giant polymer nanosheets composed of biocompatible polysaccharides. A huge aspect ratio, in excess of 10^6, is particularly applicable for novel surgical dressings. These biocompatible polymer nanosheets having heterosurfaces can thus be regarded as new biomaterials for minimally invasive treatment.

Keywords: polymers; nanosheets; biodegradable; biomaterials; polysaccharides; self-assembled monolayers; layer-by-layer; albumin; latex beads; surface modification.

INTRODUCTION

In recent years, much attention has been paid to a minimally invasive treatment in clinical aspects in the development of novel biomaterials. For example, in internal medicine, drug delivery systems (DDSs) have been developed as a new pharmacological approach to improve the efficacy and safety of drugs, and wound dressings in surgery have also been attracting many researchers to fabricate biomaterials with high safety.

In DDSs, vesicles, micelles, emulsions, and biodegradable nanoparticles have been extensively studied as carriers for biologically active substances such as drugs, recognition proteins, enzymes, genes, etc. [1]. There are two concepts for the development of DDSs—passive and active targeting systems. In the latter case, recognition proteins such as antibodies and various ligands are conjugated to the surface of the carriers to target the tissue epitopes or specific cells. In our laboratory, we have developed biocompatible and biodegradable nanoparticles such as albumin-based nanoparticles [2–5] and vesicles [6,7] carrying recombinant fragments of platelet membrane proteins [3,4,6,8] and dodeca-

*Paper based on a presentation at the 3rd International Symposium on Novel Materials and Their Synthesis (NMS-III) and the 17th International Symposium on Fine Chemistry and Functional Polymers (FCFP-XVII), 17–21 October 2007, Shanghai, China. Other presentations are published in this issue, pp. 2231–2563.
‡Corresponding author

peptide derived from fibrinogen as a recognition site for activated platelets [2,5,7,9]. These nanoparticles specifically recognize the site of bleeding injury or activated platelets. In our approach to the conjugation of high- or low-molecular-weight molecules such as glycoprotein Ibα and dodecapeptide to the surface of the particle, we observed that the activity of dodecapeptide was suppressed by the steric hindrance of the glycoprotein Ibα, and found that a spacer such as a poly(ethylene glycol) chain was needed in the conjugation of the peptides [8]. On the other hand, sheet-shaped carriers, having both obverse and reverse surfaces, have several advantages over spherical-shaped carriers because they have a larger contact area for targeting, bilateral structures leading to heterofuctionality by surface modification, and unique dynamics caused by high flexibility (Fig. 1).

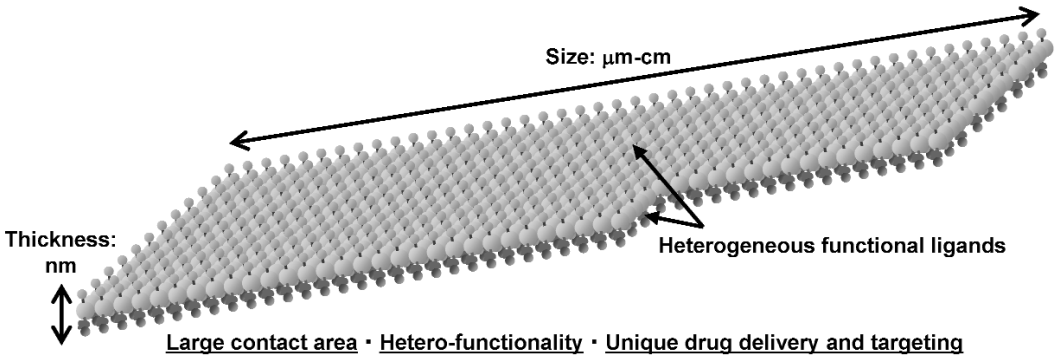

Fig. 1 General features of a free-standing nanosheet.

Hence, the sheet-shaped carriers conducted into DDSs are expected to provide suitable matrices or scaffolds for platelet adhesion (Fig. 2a). Furthermore, the idea of sheet-shaped carriers can spread to the construction of sealing biomaterials, such as materials for surgical wound dressing, if the overall size of the nanosheets is sufficiently large to cover the targeting skin or organs (Fig. 2b).

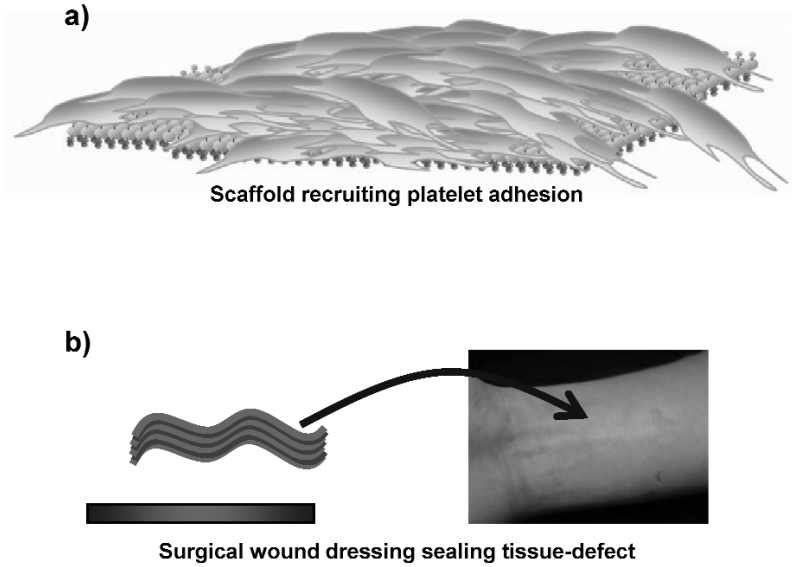

Fig. 2 Biomedical application of nanosheets: (a) platelet substitutes as a scaffold recruiting platelet adhesion and (b) an adhesive plaster for wound dressing.

Key techniques for construction of the sheet-shaped carriers are conventional surface technologies such as cast films [10], layer-by-layer (LbL) assemblies of polyelectolyte multilayers [11–15], cross-linked amphiphilic Langmuir–Blodgett films [16], self-assembled monolayers (SAMs) [17,18], and assemblies of triblock copolymers [19]. Particularly, we focus on the methodology of smart macromolecular assembling systems such as SAMs and LbL methods in order to obtain free-standing nanoscale sheets in a simple way.

In this paper, we report two types of novel sheet-shaped biomaterials that are biocompatible and biodegradable. There have been no prior reports on the potential biomedical applications of free-standing nanosheets as far as we know. With clinical applications such as DDSs in internal medicine and wound dressing in surgery particularly in mind, we describe that one type is an injectable nanosheet with a sheet-shape similar to that of native platelet, as a conceptual platelet substitute, and the other is a giant nanosheet with a huge aspect ratio, in excess of 10^6, which can be transferred onto human skin or organs, and can thus serve as nanoadhesive plasters.

NANOSHEETS IN MICROMETER SIZE FOR PLATELET SUBSTITUTES

Fabrication of free-standing nanosheets derived from proteins and nanoparticles

Organosilane SAMs have been widely applied to control physical and chemical properties of the surfaces of glass, quartz, SiO_2/Si wafers, or silica particles [20]. Furthermore, they are excellent tools to study the immobilization of proteins such as redox proteins [21], enzymes [22], and immunoglobulins using covalent or noncovalent bonds such as ionic or hydrogen bonds, van der Waals interaction, and hydrophobic interaction with the various terminal groups of SAMs. Generally, it is easy to construct patterned SAMs with uniform sizes and shapes on silicon oxide or gold substrates using a conventional photolithography processes [23]. This approach is used for the electrochemical analysis of proteins immobilized by adsorption on the substrates. On the other hand, two-dimensional patterns with steady repeatability in the particle array have also been achieved by site-selective deposition using chemical bonding or electrostatic interaction [24], an electrophotography method [25], a micromold method and gravity [26], a micromold method and a lateral capillary force [27], a patterned Au film, and a drying process of a colloidal solution onto the patterned Au film [28]. Furthermore, a novel method for deposition of a close-packed particle monolayer onto a patterned hydrophilic SAM was also recently reported using a liquid mold of which the drying process was also described [29]. However, there is no report on the preparation of free-standing proteins or nanoparticle-based nanosheets having uniform micrometer shape, nanometer thickness, and heterogenous surfaces, for use as sheet-shaped carriers.

Here, using the patterned SAMs as a template for fabrication of the nanosheet, we proposed a novel method to fabricate a free-standing nanosheet having heterosurfaces by a combination of four processes: (1) specific adsorption and two-dimensional cross-linking of proteins or nanoparticles on a patterned octadecyltrimethoxysilane SAM region (ODS-SAM); (2) surface-modification (obverse side) of the resulting nanosheet; (3) detachment from the ODS-SAM using surfactant and water-soluble sacrificial layer; and (4) surface-modification (reverse side) (Fig. 3). We selected recombinant human serum albumin (rHSA) and latex beads as model components of the nanosheet by follows.

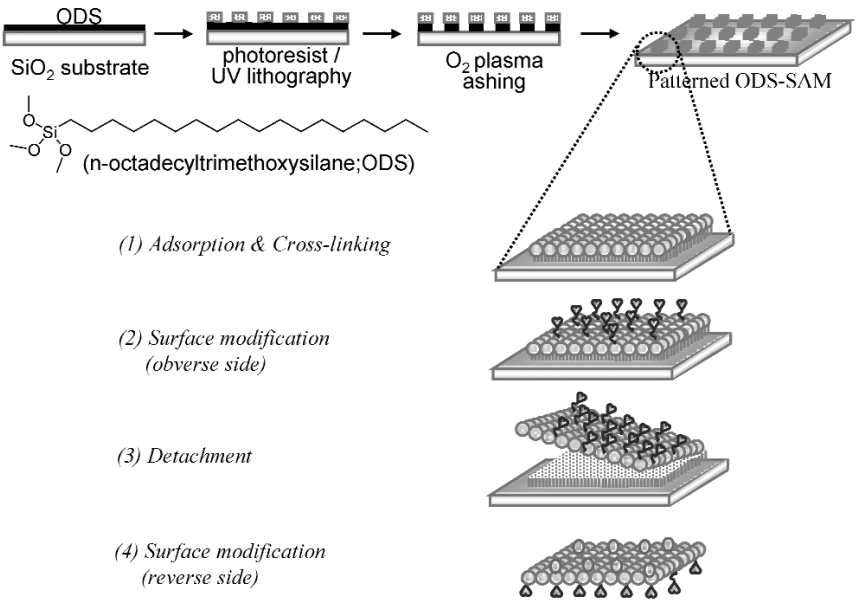

Fig. 3 Fabrication processes of free-standing nanosheets having heterosurfaces.

Free-standing albumin nanosheets [30]

In order to cross-link rHSA on the patterned ODS-SAM, we bound thiol groups to rHSA molecules (SH-rHSA, 7.4 ± 1.2 SH groups per one rHSA molecule). When the substrate of the rectangle-patterned ODS-SAM was immersed in an acetate buffer solution (pH 5.0) of the tetramethylrhodamine isothiocyanate (TRITC)-labeled SH-rHSA at a concentration of 1 μg/mL, the rectangular patterns (10×30 μm) were completely and selectively stained as shown in Fig. 4a. After removing the nonadsorbed SH-rHSA by washing with an acetate buffer solution, the SH-rHSA molecules adsorbed on the patterned ODS-SAM were cross-linked at pH 5.0 in the presence of 1 μM copper ion (II), and then immersed in a 1 % deca(oxyethylene) dodecyl ether ($C_{12}E_{10}$) solution to detach the rectangles from the substrate (Fig. 4b). Next, we dropped the solution of the rectangular sheets onto a glass plate and observed the surface of the plate using a confocal laser scanning microscopy. There were abundant rectangular rHSA nanosheets in various conformations; in particular, the curled form of the rHSA nanosheets was successfully observed in the three-dimensional images (Fig. 4c), demonstrating the high shape-stability and high flexibility and tough nature of the rHSA nanosheets.

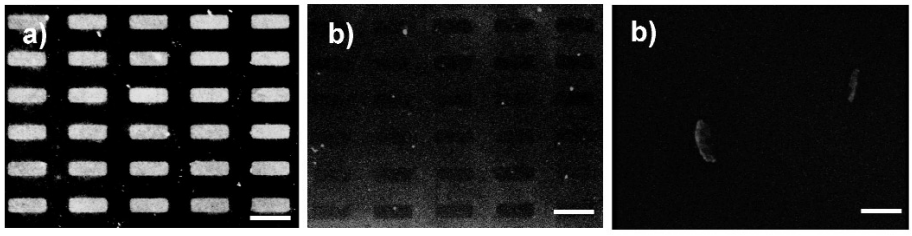

Fig. 4 Fluorescent microscopic images of (a) SH-rHSA adsorbed onto the patterned ODS-SAM and (b) the patterned ODS-SAM after $C_{12}E_{10}$ treatment. (c) Observation of the free-standing rHSA nanosheets detached from the patterned ODS-SAM using confocal laser fluorescent microscopy. Scale bars show 30 μm.

To establish the morphological detail and the thickness of the rHSA nanosheets, the nanosheets on the patterned ODS-SAM were observed by atomic force microscopy (AFM). The rectangular patterns (10×30 μm) were vividly embossed by rHSA, and nonspecific adsorption of rHSA was scarcely observed on the SiO_2 regions. From the AFM cross-sectional image, the thickness of the rHSA nanosheets plus the ODS-SAM was estimated to be 6.6 ± 1.0 nm. On the other hand, the thickness of the ODS-SAM itself was estimated to be 2.1 ± 0.7 nm. Based on the difference between both thicknesses, the thickness of the rHSA nanosheets was calculated to be 4.5 ± 1.0 nm, which agrees with the dimensions of rHSA.

We tried to modify the surface of the resulting nanosheet with latex beads, which were useful carriers because of their uniform size and ease of confirmation by microscopic observation. The NBD-labeled latex beads were conjugated onto the obverse side of the TRITC-labeled rHSA nanosheets, which had been adsorbed on the ODS-SAM and demonstrated the preparation of nanosheets having heterosurfaces. Surprisingly, there were no broken sheets, suggesting that the rHSA nanosheet-labeled latex beads possess high shape-stability and flexibility. Focusing on the nanosheet having a bent form (Fig. 5), when the rhodamine-labeled sheets were excited at 543 nm, the entire sheet turned red with a measured emission wavelength of over 570 nm. On the other hand, we tried to detect the NBD on the surface of the sheet as yellow at the excitation of 458 nm and at the emission wavelength region from 500 to 530 nm. We could confirm that the obverse surface of the sheet colored yellow, and the reverse side (bent side) was significantly quenched. Based on the above information and judging from the thickness of the rHSA nanosheet, the quenching of the NBD emission from the bent side of the nanosheet was caused by fluorescence resonance energy transfer (FRET) effect from NBD to rhodamine. It also indicates that the NBD latex beads are attached only to the obverse side of the nanosheet.

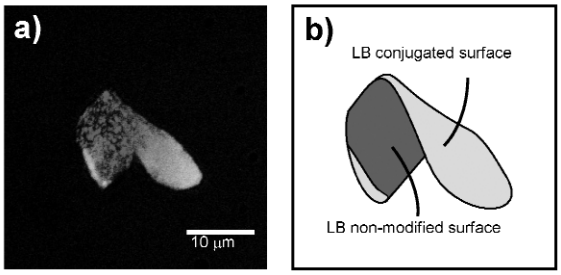

Fig. 5 (a) Confocal laser scanning microscopic images and (b) schematic image of rhodamine-labeled rHSA nanosheets, of which the obverse sides were modified with NBD-labeled latex beads.

Free-standing nanoparticle-fused nanosheets [31]

Latex beads (ϕ 100 nm) as model particles were coated with rHSA molecules to stabilize their dispersion states, to avoid nonspecific binding of the latex beads to the substrate, and to be able to conjugate various molecules to the amino groups of rHSA. A conventional dry patterning process was adopted for the specified adsorption of the rHSA latex beads onto the patterned ODS-SAM as follows. When the dispersion of the latex beads (1.0×10^{11}/mL, pH 5.0) was applied to the substrate and the suspension remaining on the substrate was then slowly blown off with a horizontal stream of N_2 gas, the latex beads were arranged as a monolayer on the entire substrate, regardless of hydrophobic and hydrophilic regions. It is possible that assembling of the latex beads would involve nucleation initiated by a capillary force and growth driven by a laminar flow to evaporate water; then the particles were forced to arrange in the form of a monolayer as previously reported [32]. Next, the immediate and repeated washing of the substrate with an acetate buffer (pH 5.0) detached the rHSA latex beads from the hydrophilic SiO_2 region, and the beads remained on the rectangular patterns of the hydrophobic dodecyl region only (5×10 μm). This indicated that the rHSA latex beads were firmly adsorbed onto the patterned

ODS-SAM by hydrophobic interaction because the net charge of the rHSA latex beads at pH 5.0, near the isoelectric point of rHSA, would be approximately zero. On the other hand, it was assumed that the rHSA latex beads were easily detached from the SiO_2 region because they were weakly attracted to the hydrophilic SiO_2 region (where the ζ-potential of the SiO_2 region at pH 5.0 was extremely negative, ca. –50 mV) [33]. After repeating the adsorption of the latex beads on the substrate plus washing, the rHSA latex beads were closely packed in a monolayer pattern as shown in Figs. 6a and 6b. The glass transition temperature (T_g) of the freeze-dried latex beads was determined as 109.9 °C by a DSC measurement in order to thermally fuse the rHSA latex beads adsorbed on the patterned ODS-SAM. The latex bead-adsorbed substrate was heated at 110 °C for 60 s on a hotplate after drying with N_2. Though the surface of the resulting sheet maintained the spherical configuration of the constituent latex beads, the neighboring latex beads were sufficiently fused as shown in Fig. 6c. When the latex bead-fused nanosheet was detached from the ODS-SAM using a poly(acrylic acid) PAA film as described below, it was confirmed that the reverse side of the nanosheet, which was directly adsorbed on the ODS-SAM, was flat and smooth, reflecting the surface morphology of the substrate.

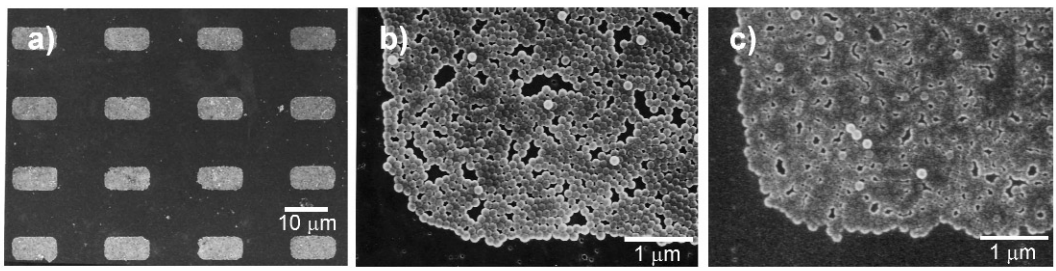

Fig. 6 (a) SEM image of rHSA-latex beads specifically adsorbed onto the patterned ODS-SAM. Magnified SEM image of rHSA-latex beads adsorbed onto the patterned ODS-SAM (b) before and (c) after thermal fusion.

PAA was used as a water-soluble sacrificial film to disperse the latex bead-fused sheets. The PAA solution was cast on the substrate where the nanosheets had been adsorbed and dried at room temperature for 15 h. It was easy to peel off the PAA film from the substrate, and the resulting film was transparent as shown in Fig. 7a. Observation of the PAA film using a scanning electron microscope (SEM) confirmed that the latex bead-fused nanosheet was completely transferred to the PAA film as shown in Fig. 7b, and no residual sheets were observed on the substrate (data not shown). Such complete transfer is possible because the ionic and/or hydrogen bonding between the PAA and the latex bead-fused nanosheets would be stronger than the van der Waals interaction of the dried nanosheets with the CH_3-terminal SAMs. In agreement with the report by Stroock et al., describing the exquisite transfer of a polymer film on a substrate to a PAA film and suspension in an aqueous buffer, their transfer mechanism has been successfully reproduced in the patterned nanosheets [34]. Furthermore, it was easy to dissolve the resulting PAA film to release the latex bead-fused nanosheet in a phosphate buffer at pH 7.4, and the free-standing nanosheets were collected on the membrane filter as shown in Fig. 7c.

It was confirmed that these nanosheets were able to maintain their rectangular shape, indicating in turn that the neighboring latex beads were sufficiently well fused to retain the two-dimensional shape.

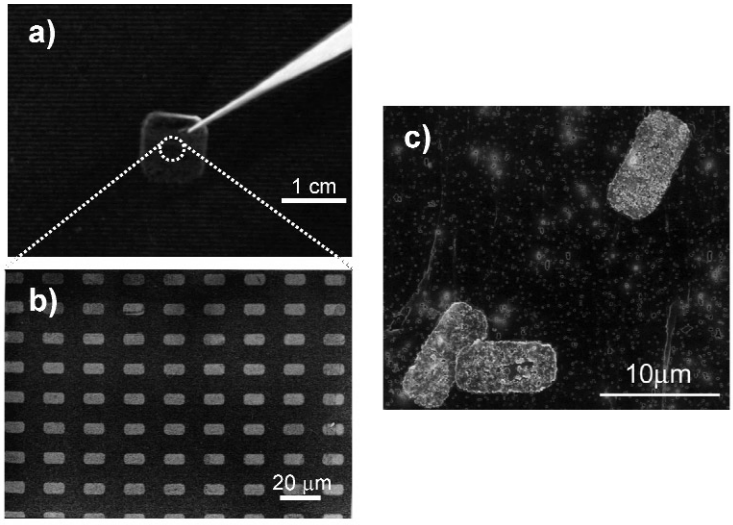

Fig. 7 (a) Photo and (b) SEM image of latex bead-fused nanosheets transferred from the ODS-SAM to the PAA film. (c) SEM image of free-standing latex bead-fused sheets after dissolution of the resulting PAA film.

Finally, when the PAA film supporting the latex bead-fused nanosheets was observed, it was easy to confirm that the reverse smooth side of the nanosheet, which had been in direct contact with the silicon substrate, emerged onto the surface of the resulting PAA film (data not shown). It is concluded that either side of the nanosheet could be selectively modified using the PAA film, not only as a tool for transference of the sheets and a sacrificial film for dispersion, but also as a supporting film for hetero-modification of the nanosheet. Two kinds of water-soluble fluorescent probes, TRITC and fluorescein isothiocyanate (FITC), were selected as model components to show hetero-modification of the nanosheet. An excess of TRITC (5 μM) was first added to the amino groups of the rHSA-adsorbing latex beads on the patterned dodecyltrimethoxysilane (DTS)-SAM. After sufficient washing with distilled water, the PAA solution was cast on the substrate and the dried PAA film was peeled off. For FITC modification of the reverse side of the nanosheets, conditions under which the PAA film would be insoluble were used: pH 4.0 and saturated sodium chloride. An excess of FITC (5 μM) was added to the reverse side of the PAA film which was then dissolved in a phosphate buffer at pH 7.4, to allow collection of latex bead-fused nanosheets coated with each of the two fluorescent labels. Using a confocal laser scanning microscope, the abundance of rectangular nanosheets was confirmed, on one or other of the two surfaces where either fluorescent probe was localized: the obverse side of the nanosheets was conjugated with TRITC and the reverse side was conjugated with FITC (Fig. 8). Thus, this study has proved that the latex bead-fused sheet was able to modify selectively either surface using the PAA film as a supporting film.

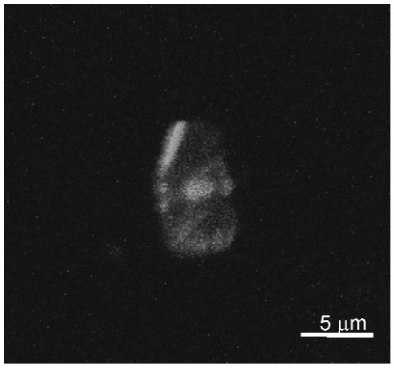

Fig. 8 Images of TRITC- and FITC-labeled latex bead-fused sheets using confocal laser fluorescence microscopy.

NANOSHEETS AS NANOADHESIVE PLASTERS

Quasi two-dimensional free-standing giant nanosheets

There have been several progressive results about methodology for the fabrication of giant nanosheets with a huge size–aspect ratio in recent nanotechnology [15,35–39]. Convenient fabrication or manipulation of nanoscale materials will significantly enhance the potential applicability of nanotechnology. One novel methodology for the fabrication of nanoscale materials involving a wide variety of macromolecules is an LbL technique [40]. The LbL method involves alternative adsorption of oppositely charged polyelectrolytes by different noncovalent linking such as electrostatic, hydrogen-bonding, or hydrophobic interactions [40–44]. Application of LbL-based materials has been explored in several fields such as electrochemical devices, chemical sensors, nanomechanical sensors, nanoscale chemical/biological reactors, and as a DDS [45]. The LbL method has been used to fabricate a free-standing ultra-thin membrane using a spin-coating assisted LbL (SA-LbL) method [46–48] (Fig. 9). The SA-LbL method can prepare ultra-thin membranes by spin-coating each polyelectrolyte alternatively on a substrate covered with a sacrificial layer. Subsequent dissolution of the sacrificial layer releases the free-standing ultra-thin membrane within several minutes, unlike conventional protocols that require many hours (e.g., dipping LbL process).

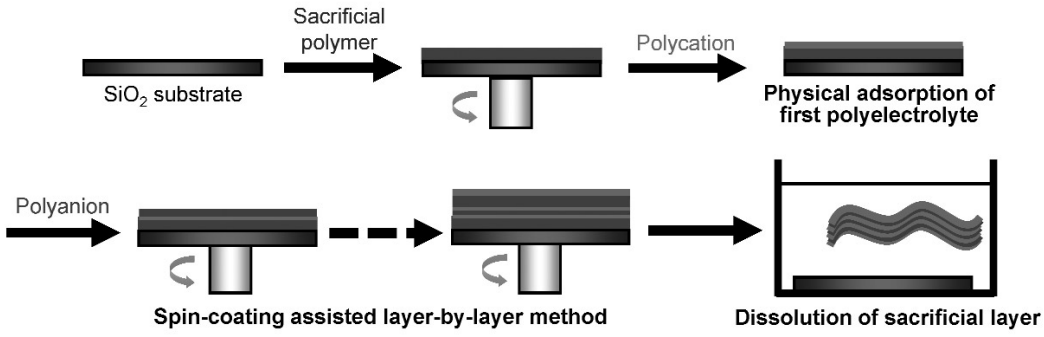

Fig. 9 Preparative scheme of free-standing nanosheets exploiting an SA-LbL method.

Because the membranes are composed of polymers with a sheet-like structure of nanometer thickness, they possess a huge aspect ratio ($\geq 10^6$ depending on the size of the substrate). As such, these structures have been referred to as "polymer nanosheets" by Miyashita [36]. The free-standing polymer nanosheets released from the substrate were composed not only by the SA-LbL method, but also by a

Langmuir–Blodgett method followed by cross-linking amphiphilic copolymers or by a sol/gel method with organic/inorganic interpenetrating networks [36,37]. These polymer nanosheets have been reported to be well-organized, compliant, and robust materials for micro/nano-mechanical studies [49–51]. However, the nanosheets based on SA-LbL were only the way for obtaining the materials without using a chemical cross-linking method but macromolecular assemblies such as electrostatic interaction, which is quite suitable for biomedical application of the nanosheets. Herein, we are exploiting an SA-LbL method for the construction of biocompatible nanosheets.

Free-standing polysaccharide nanosheets [52]

In order to fabricate the nanosheet, we use chitosan and sodium alginate (Na alginate), which have amino and carboxylic groups as cationic and anionic polyelectrolytes at ambient pH (Fig. 10). These polysaccharides are used in biomedical fields such as wound dressing and artificial skin because of their high biocompatibility and biodegradability.

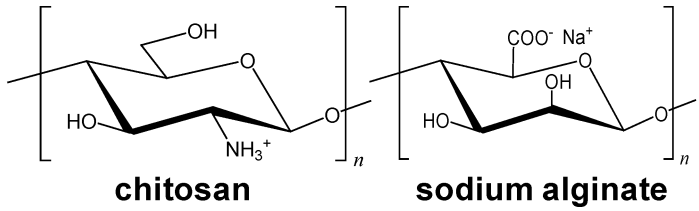

Fig. 10 Chemical structures of biocompatible polysaccharides.

Then, following the SA-LbL method as mentioned above, we obtained a free-standing nanosheet consisting of polysaccharides (i.e., polysaccharide nanosheet). For the morphological study of the polysaccharide nanosheet surface, the free-standing nanosheet floating in acetone was transferred onto a fresh silicon wafer and observed by AFM. Large-scale (90×90 μm) topographic images revealed that the nanosheet surface was as smooth and flat as the silicon wafer surface without any corrugations and wrinkles. From the cross-sectional analysis of the nanosheet edge, the thickness of the nanosheet with 10.5 layer pairs of polysaccharides was estimated to be 30.2 ± 4.3 nm, corresponding to the ellipsometric thickness of the polysaccharide ultra-thin film directly assembled on the SiO_2 substrate (Fig. 11a). These topographical results were obtained due to the high-speed horizontal diffusion of the polymers during spin-coating. Because the morphology of the polysaccharide nanosheet was quite smooth and flat, the adsorbed nanosheets on the SiO_2 substrate showed a brilliant color change depending on the adsorbed number of the nanosheet (Fig. 11b).

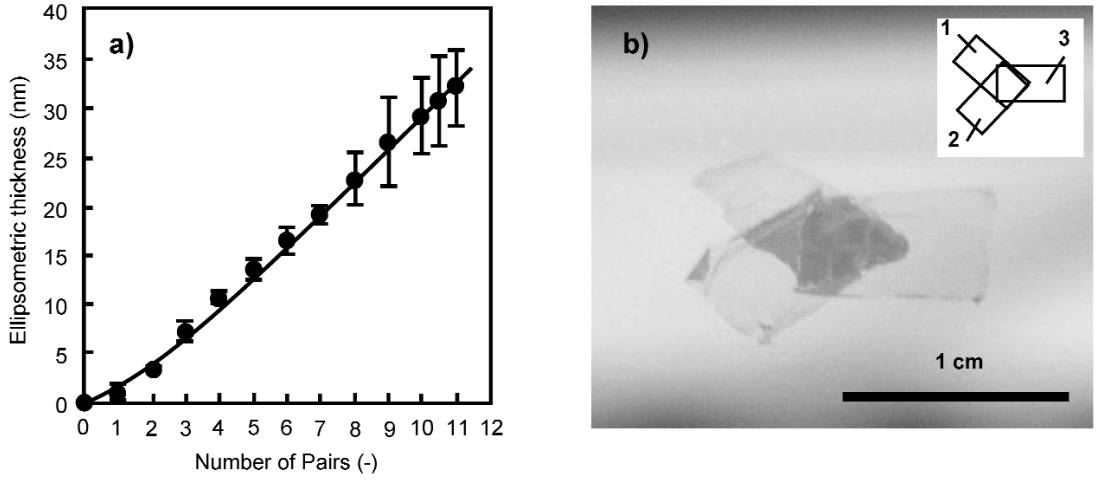

Fig. 11 Morphological study of polysaccharide nanosheets: (a) increment of the thickness investigated by ellipsometry and (b) triple adsorbed polysaccharide nanosheets (inset: an illustration of the adsorption order) on a SiO_2 substrate.

Nanoadhesive plaster including ubiquitous transference of the nanosheets

In order to transfer the polysaccharide nanosheet from the surface of one substrate to another without distorting the overall shape, we used a water-soluble sacrificial membrane as a substrate of the polysaccharide nanosheet because giant free-standing nanosheets in the liquid tended to be overwhelmed in the air due to a huge size–aspect ratio. Here, we named this layered composite film a "nanoadhesive plaster" because the nanosheet could attach to skin or organ and the water-soluble membrane was finally dissolved (Fig. 12).

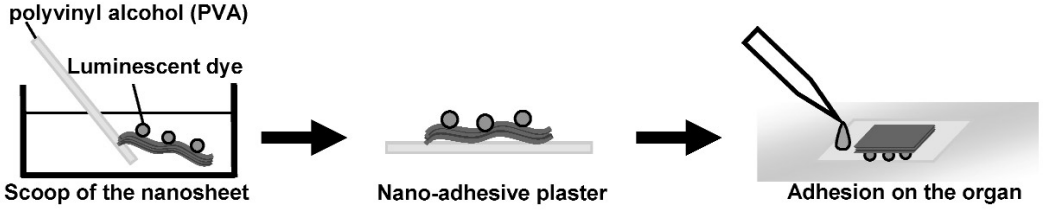

Fig. 12 Practical working design of nanoadhesive plaster onto the organ.

In order to transfer the polysaccharide nanosheet from the substrate onto skin or organ, we prepared a poly(vinyl alcohol) (PVA) membrane as a hydrophilic sacrificial membrane. We chose PVA as a suitable material for the sacrificial membrane because it is a water-soluble polymer that does not adversely affect the living body. The PVA membrane was prepared by casting of a concentrated 10 wt % PVA aqueous solution on a SiO_2 substrate. The PVA membrane, approximately 70-μm thickness, can be pealed from the solid substrate. The free-standing PVA membrane was robust and compliant in acetone when picked up with tweezers. With the resulting PVA membrane, the polysaccharide nanosheet, modified with a small amount of commercialized luminescent pigment for ease of visibility in the dark, was scooped onto the air-solid surface. A luminescent-labeled nanosheet was clearly observed in the dark as a square shape. No cracks or deformations were observed in the nanosheet over a period of a few months at the ambient temperature.

To test the practical applications of the nanoadhesive plaster, we attached it to the cecum of a living rat. The adhesion of the polysaccharide nanosheet supported by the water-soluble PVA membrane was observed from the luminescent signals (Fig. 13a). Then the PVA membrane was dissolved with a few mL drops of saline through the syringe. Luminescent signals from the modified nanosheet confirmed that the shape and size of the polysaccharide nanosheet were preserved on the cecum. Furthermore, the overall shape of the polysaccharide nanosheet was completely fitted on the surface relief of the organ due to high flexibility of the nanosheet and occurrence of the firm tissue-adhesion due to the polysaccharide nanosheet was not observed (Fig. 13b). These results indicated that the polysaccharide nanosheet was successfully transferred onto the tissue surface by dissolution of the PVA membrane and quite stable on the tissue surface. Moreover, the nanoadhesive plaster was applicable for the skin surface [52]. We predict that free-standing polymer nanosheet has potential biomedical application as unique surgical or cosmetic materials.

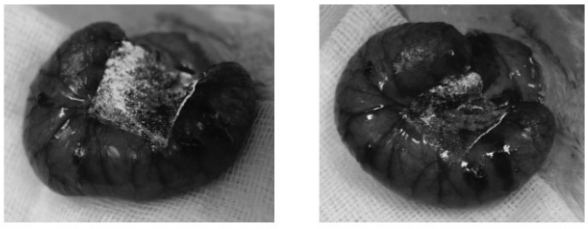

Fig. 13 Nanoadhesive plaster on rat cecum: (a) before and (b) after dissolution of the supported PVA membrane.

CONCLUDING REMARKS

We succeeded in preparing two types of free-standing nanosheet, envisaging biomedical application. One is an injectable nanosheet as platelet substitutes, with the sheet shape similar to native platelets in the concept of platelet substitutes, which was constructed on the micropatterned substrate. The other is a giant nanosheet constructed by LbL assembly with a huge size–aspect ratio over 10^6, customized to nanoadhesive plasters which were ubiquitously transferred by the polysaccharide nanosheet onto human skin or organ. Now, we have opened the potential applicability of the polymer nanosheet in the biomedical fields from the fundamental materials science, which will divert to the new methodology of minimal-invasive treatments in clinical aspects.

ACKNOWLEDGMENTS

This work was supported by Global COE "Practical Chemical Wisdom" and "Consolidated Research Institute for Advanced Science and Medical Care" from MEXT, and the Shorai Foundation for Science and Technology (S. T.), Japan. T. F. was the scholar "Doctor-21" of the Yoshida Scholarship Foundation. Y. O. was a recipient of the Japan Health Sciences Foundation.

REFERENCES

1. Y. Tomii. *Curr. Pharm. Des.* **8**, 467 (2002).
2. S. Takeoka, Y. Teramura, Y. Okamura, M. Handa, Y. Ikeda, E. Tsuchida. *Biomacromolecules* **2**, 1192 (2001).
3. S. Takeoka, Y. Teramura, H. Ohkawa, Y. Ikeda, E. Tsuchida. *Biomacromolecules* **1**, 290 (2000).
4. Y. Teramura, Y. Okamura, S. Takeoka, H. Tsuchiyama, H. Narumi, M. Kainoh, M. Handa, Y. Ikeda, E. Tsuchida. *Biochem. Biophys. Res. Commun.* **306**, 256 (2003).

5. Y. Okamura, S. Takeoka, Y. Teramura, Y. Maruyama, E. Tsuchida, M. Handa, Y. Ikeda. *Transfusion* **45**, 1221 (2005).
6. S. Takeoka, Y. Teramura, Y. Okamura, E. Tsuchida, M. Handa, Y. Ikeda. *Biochem. Biophys. Res. Commun.* **296**, 765 (2002).
7. Y. Okamura, I. Maekawa, Y. Teramura, Y. Maruyama, E. Tsuchida, M. Handa, Y. Ikeda, S. Takeoka. *Bioconjugate Chem.* **16**, 1589 (2005).
8. Y. Okamura, M. Handa, H. Suzuki, Y. Ikeda, S. Takeoka. *J. Artif. Organs* **9**, 251 (2006).
9. S. Takeoka, Y. Okamura, Y. Teramura, N. Watanabe, H. Suzuki, E. Tsuchida, M. Handa, Y. Ikeda. *Biochem. Biophys. Res. Commun.* **312**, 773 (2003).
10. J. Mattson, J. A. Forrest, L. Borjesson. *Phys. Rev. E* **62**, 5187 (2000).
11. Z. Tang, N. A. Kotov, S. Magonov, B. Ozturk. *Nat. Mater.* **2**, 413 (2003).
12. F. Mallwitz, A. Laschewsky. *Adv. Mater.* **17**, 1296 (2005).
13. A. Mamedov, N. A. Kotov, M. Prato, D. M. Guldi, J. P. Wicksted, A. Hirsch. *Nat. Mater.* **1**, 190 (2002).
14. W. T. Huck, A. D. Stroock, G. M. Whitesides. *Angew. Chem., Int. Ed.* **39**, 1058 (2000).
15. A. A. Mamedov, N. A. Kotov. *Langmuir* **16**, 5530 (2000).
16. F. Mallwitz, W. A. Goedel. *Angew. Chem., Int. Ed.* **40**, 2645 (2001).
17. W. Eck, A. Küller, M. Grunze, B. Völkel, A. Gölzhäuser. *Adv. Mater*. **17**, 2583 (2005).
18. H. Xu, W. A. Goedel. *Langmuir* **18**, 2363 (2002).
19. C. Nardin, M. Winterhalter, W. Meier. *Langmuir* **16**, 7708 (2000).
20. A. Ulman. *An Introduction to Ultrathin Organic Films from Langmuir–Blodgett to Self-Assembly*, Academic Press, San Diego (1991).
21. D. E. Khoshtariya, J. Wei, H. Liu, H. Yue, D. H. Waldeck. *J. Am. Chem. Soc.* **125**, 7704 (2003).
22. E. E. Ferapontova, S. Shipovskov, L. Gorton. *Biosens. Bioelectron.* **22**, 2508 (2007).
23. D. Niwa, Y. Yamada, T. Homma, T. Osaka. *J. Phys. Chem. B* **108**, 3240 (2004).
24. Y. Masuda, W. S. Seo, K. Koumoto. *Jpn. J. Appl. Phys.* **39**, 4596 (2000).
25. H. Fudouzi, M. Kobayashi, M. Egashira, N. Shinya. *Adv. Powder Technol.* **8**, 251 (1997).
26. W. J. Wen, N. Wang, D. W. Zheng, C. Chen, K. N. Tu. *J. Mater. Res.* **14**, 1186 (1999).
27. Y. Sun, G. C. Walker. *J. Phys. Chem. B* **106**, 2217 (2002).
28. Q. Guo, C. Arnoux, R. E. Palmer. *Langmuir* **17**, 7150 (2001).
29. Y. Masuda, K. Tomimoto, K. Koumoto. *Langmuir* **19**, 5179 (2003).
30. Y. Okamura, T. Goto, D. Niwa, Y. Fukui, M. Otsuka, N. Motohashi, T. Osaka, S. Takeoka. *J. Biomed. Mater. Res. A* (2008). In press.
31. Y. Okamura, S. Utsunomiya, H. Suzuki, D. Niwa, T. Osaka, S. Takeoka. *Colloids Surf., A* **318**, 184 (2008).
32. N. D. Denkov, O. D. Velev, P. A. Kralchevsky, I. B. Ivanov, H. Yoshimura, K. Nagayama. *Langmuir* **8**, 3183 (1992).
33. A. Hozumi, S. Asakura, A. Fuwa, N. Shirahata, T. Kameyama. *Langmuir* **21**, 8234 (2005).
34. A. D. Stroock, R. S. Kane, M. Weck, S. J. Metallo, G. M. Whitesides. *Langmuir* **19**, 2466 (2003).
35. C. Jiang, S. Markutsya, Y. Pikus, V. V. Tsukruk. *Nat. Mater.* **3**, 721 (2004).
36. Y. Kado, M. Mitsuishi, T. Miyashita. *Adv. Mater*. **17**, 1857 (2005).
37. R. Vendamme, S. Onoue, A. Nakao, T. Kunitake. *Nat. Mater*. **5**, 494 (2006).
38. H. Endo, Y. Kado, M. Mitsuishi, T. Miyashita. *Macromolecules* **39**, 5559 (2006).
39. S. S. Ono, G. Decher. *Nano Lett*. **6**, 592 (2006).
40. Y. Lvov, G. Decher, H. Mohwald. *Langmuir* **9**, 481 (1993).
41. Y. Lvov, K. Ariga, I. Ichonose, T. Kunitake. *J. Am. Chem. Soc.* **117**, 6117 (1995).
42. G. Decher, Y. Lvov, J. Schmitt. *Thin Solid Films* **244**, 772 (1994).
43. V. V. Tsukruk, V. N. Bliznyuk, D. Visser, A. L. Campbell, T. J. Buning, W. W. Adams. *Macromolecules* **30**, 6615 (1997).
44. G. Decher. *Science* **277**, 1232 (1997).

45. G. Decher, J. B. Schlenoff. *Multilayer Thin Films*, Wiley-VCH, Weinheim (2003).
46. J. Cho, K. Char, J. Hong, K. Lee. *Adv. Mater.* **13**, 1076 (2001).
47. J. Cho, K. Char. *Langmuir* **20**, 4011 (2004).
48. C. Jiang, S. Markutsya, V. V. Tsukruk. *Adv. Mater.* **16**, 157 (2004).
49. S. Markutuya, C. Jiang, Y. Pikus, V. V. Tsukruk. *Adv. Funct. Mater*. **15**, 771 (2005).
50. C. Jiang, S. Singamaneni, E. Merrick, V. V. Tsukruk. *Nano Lett*. **6**, 2254 (2006).
51. C. Jiang, M. E. McConney, S. Singamaneni, E. Merrick, Y. Chen, J. Zhao, L. Zhang, V. V. Tsukruk. *Chem. Mater*. **18**, 2632 (2006).
52. T. Fujie, Y. Okamura, S. Takeoka. *Adv. Mater.* **19**, 3549 (2007).